Enhancing hydrogen peroxide activation in heterogeneous Fenton reaction by codoping hydrochar with iron and Copper

Abderrazzak Adachi [a], Faiçal El Ouadrhiri [a,*], Ebraheem Abdu Musad Saleh [d], Fatima Moussaoui [a], Raed H. Althomali [d], Soukaina El Bourachdi [a], Kakul Husain [d], Abdelmajid Faris [b], Ismail Hassan [d], Khalil Azzaoui [a,c], Belkheir Hammouti [c], Amal Lahkimi [a]

[a] *Laboratory of Engineering, Electrochemistry, Modelling and Environment, Faculty of Sciences Dhar El Mahraz, Sidi Mohamed Ben Abdelah University, Fez, Morocco*
[b] *Laboratory of Molecular Chemistry, Department of Chemistry, Faculty of Sciences Semlalia, Cadi Ayyad University, P.O. Box 2390, 40001 Marrakech, Morocco*
[c] *Euro Mediterranean University of Fez, Fez, Morocco*
[d] *Chemistry Department, College of Arts & Science, Prince Sattam Bin Abdulaziz University, Wadi Al-Dawaser, Alkharj, Saudi Arabia*

A R T I C L E   I N F O

A B S T R A C T

The development of a bimetallic Fenton-type catalyst with desirable activity and reusability remains a major challenge for the practical degradation of organic pollutants. Herein, we focused on modifying almond shell hydrochar with a Fe/Cu bimetal (Fe/Cu-HC) to develop a catalyst capable of activating H_2O_2 for degrading MO. The bimetallic Fe/Cu-HC catalyst was synthesized through hydrothermal carbonization and pyrolysis and characterized using SEM, FTIR, BET analysis, and XRD to confirm the presence and uniform dispersion of Cu and Fe co-doped species on HC. The impact of various factors, such as the solution pH (X_1), organic pollutant concentration (X_2) and catalyst mass (X_3), on dye degradation efficiency via heterogeneous Fenton oxidation, was examined using the BBD model coupled with Surface response methodology (RSM). The Fe/Cu-HC catalyst showed superior performance in degrading MO dye compared to single-metal catalysts (Cu-HC, Fe-HC), due to the synergistic interaction between Fe and Cu species. To demonstrate the heterogeneous Fenton catalytic performance of the synthesized FeCu/HC, the results showed that 98.97 % of methyl orange was eliminated under optimal conditions: 100 mg. l^{-1} of methyl orange, a duration of 1 h, a catalyst mass of 1.65 g. l^{-1}, a pH of 6, and a concentration of 4 mM H_2O_2. In addition, the Fe/Cu-HC catalyst showed excellent stability over multiple cycles, with minimal metal leaching. These results indicate that Fe/Cu-HC is a promising catalyst for the degradation of methyl orange and pave the way for the development of other cost-effective and efficient bimetallic catalysts for environmental remediation.

1. Introduction

Today, water pollution is considered as a big problem, affecting the lives of individuals and the economic development of countries (Fu et al., 2021). Among these, wastewater from the textile industry poses a major challenge for environmental protection because of its complex composition, strong coloration, extreme toxicity and persistence (Shi et al., 2018). Methyl orange (MO) is frequently used in the textile, cosmetics, and paint industries. However, due to its anionic nature and membership of the azo group (N = N), it is potentially hazardous to the aquatic environment (Peerakiatkhajohn et al., 2021). Frequently it is used in the wastewater treatment processes as adsorption, coagulation-flocculation and advanced oxidation processes (AOP) (Adachi et al., 2023); (Adachi, 2023) ; (Khan, 2023) . In contrast to conventional water treatment methods, AOP process have been identified as a promising and efficient technology for breaking down harmful contaminants (El Ouadrhiri, May 2023), AOPs based on OH⁻ radicals are considered as a reliable approach for the degradation of methyl orange (MO), given their higher oxidation potential (E^0 = 2.80 V) (Wang et al., 2020). Accordingly, it is possible to activate hydrogen peroxide H_2O_2, using ultrasound (Rahdar et al., 2019), ultraviolet (Santos et al., 2020), heat treatments (Mirdamadi et al., 2022), and transition metal-based materials (Lousada et al., 2012). It was found that transition metals, such as Cu, Fe, and Co exhibited higher efficiency in the activation of hydrogen

peroxide which makes them a subject of numerous research. In fact, iron and copper have attracted greater importance for ecological and economic reasons (Song et al., 2021); (Ding, 2020) . But in terms of efficiency, single metal oxides exhibited less efficiency compared with bimetal oxides, in particular iron/copper dioxide. Those later have a significantly higher activation efficiency (Xie, 2023); (Binh et al., 2020) . With regard to the standard redox potential comparison between copper and iron, copper can promote valence cycling and electron exchange, consequently enhancing the activation capacity of the heterogeneous Fenton catalyst (Tang and Wang, 2020). Moreover, Zhenlu Li *et al.* demonstrated that 99 % of methylene blue (MB) was eliminated by the catalyst Cu/CuFe$_2$O$_4$ (Li et al., 2018), which was significantly superior to that of Cu/ZrO$_2$ (92 %) and Fe$_2$O$_3$ (90 %) (Hussain et al., 2022); (Baldrian, 2006) . These Fenton catalysts were characterized by heavy metal leaching and they require very acidic pH operating conditions, resulting in secondary pollution during the water treatment process (Duan, 2020). To overcome this challenge, other approaches consists on the to use carbonaceous materials as supports to prevent metal leaching and neutralize the pH of the solution, such as graphene (Duan et al., 2016), carbon nanotubes (Li et al., 2020), biochar (Babar, 2022) and hydrochar (Wang et al., 2020). Compared with carbon-based materials, hydrochar (HC) possesses rich surface functional groups, a low cost, eco-friendly, porous, recyclable structure (Genli et al., 2022). As a result, hydrochar (HC) produced by the hydrothermal carbonization (HTC) method from various biomass presents a diverse range of catalytic properties (Roman et al., 2021). A hydrochar modified with transition metals was used to produce a solid catalyst, aiming to improve their catalytic efficiency in the heterogeneous Fenton process (Li, 2022). Huang *et al.* prepared a solid catalyst CuFe$_2$O$_4$@BC based on eucalyptus sawdust and reported a malachite green degradation efficiency of up to 98.9 % (Huang, 2021). To date, the catalytic performance of almond shell hydrochar modified with Fe/Cu bimetallic oxides has been seldom reported, and its enhanced efficiency in the presence of H$_2$O$_2$ remains undetermined (Ledesma et al., 2018). In this study, we produced a hydrochar (support) derived from almond shells (AS) and co-doped with iron and copper using the hydrothermal carbonization (HTC) method. This material was designed to activate hydrogen peroxide (H$_2$O$_2$) to degrade various organic pollutants. The main objective of this research is to determine the efficiency and mechanisms of this catalyst under optimal conditions, to better understand its potential for environmental remediation applications. AS has been widely generated throughout the world. According to data from the International Nut Foundation, almond shell production for the 2017–2018 season increased to around 1.2 million tons (Queirós, 2019). Almond shells, classified as solid waste containing some cellulose, lignin, silica and carbohydrates, found in abundance, with low cost and readily available (Hashemian et al., 2014). Herein, a bimetallic FeCu co-doped hydrochar from AS (Fe/Cu-HC) catalyst was synthesized through a wet impregnation process followed by pyrolysis. The primary objectives were as follows: i) to prepare catalysts based on hydrochar doped with iron (Fe-HC), copper (Cu-HC), and bimetallic co-doped (Fe/Cu-HC) derived from AS. ii) to study the physical and chemical characterization of the FeCu co-doped bimetallic catalyst. iii) to test the catalytic performance of Fe/Cu-HC using the H$_2$O$_2$ system. iv) to optimize the heterogeneous Fenton process using the Box-Behnken design. Our approach, applied in this research, demonstrates and opens up a new, simple and highly interesting route through the use of (AS) as a source of hydrochar for the synthesis of efficient catalysts for wastewater treatment.

2. Materials and methods

2.1. Raw materials

The AS were collected from an industrial plant in Fes City in Morocco. They were rinsed with demineralized water to eliminate surface contamination and pulp residues, then dried at 100 °C for 12 h.

After drying, the AS were grounded to retain only the shell structure, which was then ground and sieved to obtain particles smaller than 250 µm, stocked as hydrochar precursors for further experiments. Trihydrate of copper nitrate (Cu (NO$_3$)$_2$, 3H$_2$O, ≥99 %), ferrous sulfate (FeSO$_4$, 7H$_2$O), hydroxide of sodium (NaOH, 99 %), and the peroxide hydrogen (H$_2$O$_2$, 30 % w/w), Hydrogen Chloride (HCl) ≥ 99 %, potassium hydroxide (KOH, ≥99 %), Methyl Orange (purity ≥ 97 %) were provided by China's Sinopharm Chemical Reagent Co., Ltd. All the compounds used in this study were of analytical quality (Adachi et al., 2023). Distilled water from an ultrapure purification system was used for all experimental solutions. The molecular composition of the methyl orange dye is also shown in Table 1.
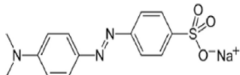
2.2. Synthesis of catalyst

Hydrochar (HC) from Almond shell was prepared, using the HTC hydrothermal carbonization method (Alcazar-Ruiz et al., 2023). Hydrothermal carbonization of AS was realized, using a 100 ml autoclave lined with polypropylene. Initially, 60 ml of distilled water with 2 g of AS powder was added to the Teflon autoclave. KOH was then added to the mixture to function as a catalyst for the hydrothermal process (Oginni et al., 2019). After careful sealing, the autoclave was placed in an oven set at 200 °C for two hours (Adachi et al., 2023). Throughout the hydrothermal carbonization process, the heating rate remained unchanged at 5 °C/min. Following the autoclave's natural cooling process, the solid was extracted using vacuum filtration, repeatedly cleaned with distilled water, and then left to dry overnight in the oven. The iron and copper-loaded hydrochar was produced using a wet impregnation process. To achieve this, a solution containing 0.1 M FeSO$_4$·7H$_2$O and 0.1 M Cu (NO$_3$)$_2$·3H$_2$O was prepared by mixing these compounds in 100 ml of ultrapure water, aiming for a Fe/Cu molar ratio of 1:1, as previously reported. This mixture was stirred for 12 h to ensure complete dissolution of the salts, then dried for 6 h at 70 °C. Subsequently, the iron and copper-doped hydrochars were subjected to pyrolysis in a muffle furnace at 500 °C for 2 h under a nitrogen atmosphere, followed by multiple washings with distilled water (Pourali et al., 2022), The resulting product is denoted as Fe/Cu-HC (Fig. 1). For comparison purposes, non-doped HC, copper-doped hydrochar (Cu-HC), and iron-doped hydrochar (Fe-HC) were also prepared using the same procedure as detailed above.

2.3. Characterizations

Analysis of the structure and crystallinity of the prepared hydrochar and co-doped catalyst (Fe/Cu-HC) was carried out using an X-ray diffractometer (X' Pert Pro) equipped with a detector operating at 40 kV and 30 mA, using Cu Kα radiation (λ = 1.540598 Å). Fourier transform infrared (FT-IR) spectroscopy (Nexus, Thermo Nicolet) was used to identify chemical bonds on the catalyst surface. Scanning electron microscopy (SEM) and BET (Brunauer, Emmett and Teller) analysis were used to examine the shape and microstructure of the Fe/Cu-HC catalyst. Mapping analysis and X-ray Energy Dispersion Spectroscopy (EDS) were carried out to confirm the presence of iron and copper in the co-doped catalyst.

Table 1
Chemical properties of the MO dye (Rehan, 2023).

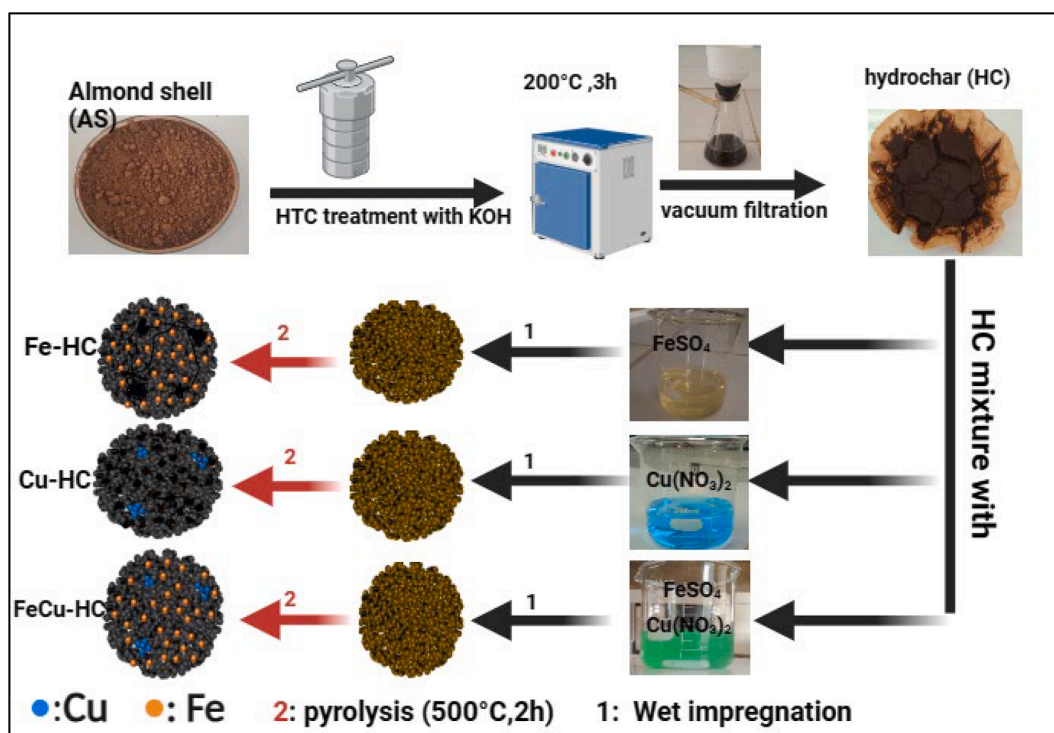| Characteristic	Methyl orange
Chemical formula	C$_{14}$H$_{14}$N$_3$NaO$_3$S
Molar weight	327.33 (g.mol^{-1})
C.A. S	547–58-0
I.C. number	13,025
λ$_{max}$	464 nm
Molecular structure	

Fig. 1. Schematic illustration of the preparation of Fe-HC, Cu-HC and Fe/Cu-HC.

2.4. Catalytic performance

Experimental batch tests were carried out in a 250 ml beaker placed on a hot plate with magnetic stirring (Stuart-SB 162) at a rotation speed of 150 rpm, as shown in Fig. 2. Each experiment utilized a working volume of 100 ml of MO dye solution, prepared by diluting the stock solution to a specific concentration. The heterogeneous Fenton reaction for MO degradation was carried out with the reaction temperature, time, and H_2O_2 dose adjusted to the optimal values discovered in a preliminary investigation conducted under the specified conditions

Fig. 2. Instrument used in the heterogeneous Fenton process.

(35.5 °C and 1 h, 4 mM, respectively) (Adachi et al., 2023). A sample containing the pollutants was taken during the one-hour oxidation process, and it was then isolated using the filtration method. This made it possible to assess and examine the concentrations of pollutants in the solution. Organic dye concentration was determined with a UV–visible spectrophotometer (2005-HJD501) using a wavelength of 464 nm (Tao et al., 2019), as shown in Fig. 1S (Ledesma et al., 2018). Pollutant degradation efficiency was evaluated using equation (1) (Pourali et al., 2022); (Naghshbandi and Gholinejad, 2023) .

$$\text{Decolorization efficiency}\,(\%) \,=\, \text{DE}\,(\%) \,=\, \left(\frac{C_0 - C_t}{C_0} \right) \times 100 \qquad (1)$$

with C_0 (mg/l) and C_t (mg/l) corresponding to the initial and final concentrations of organic pollutants respectively.

2.5. Experimental design

The response surface methodology (RSM) is a powerful tool for the optimization and statistical analysis of experimental data. It is especially valuable for optimization because it allows for the simultaneous consideration of multiple parameters (Methods, 2010). When combined with the Box-Behnken design (BBD), RSM provides comprehensive conclusions and detailed information with a reduced number of experiments, highlighting the interactive effects of operational parameters on the response. The Box-Behnken (BBD) design model has been applied to optimize the pH of the solution, the organic pollutant concentration MO and the mass of the catalyst (Fe/Cu-HC), and to assess the relationship between these parameters. The BBD required 15 tests, in which the three parameters were coded in three levels, varying in the following intervals: pH of the solution ($X_1 = 3$ to 6), concentration of the organic pollutant MO ($X_2 = 20$ to 100 mg. l^{-1}), mass of the Fe/Cu-HC catalyst ($X_3 = 1$ to 2 g.l^{-1}). The model coefficient in quadratic terms was then calculated using these three variables (Table S1). The MO degrading efficiency is represented by the anticipated reaction, Y_i

$$Yi = \beta 0 + \sum_{i=1}^{n} \left(\beta_i X_i \right) + \sum_{i=1}^{n} \left(\beta_{ii} X_i^2 \right) + \sum_{i=1}^{n-1} \sum_{j=1}^{n} \left(\beta_{ij} X_i X_j \right) + \mathscr{E} \qquad (2)$$

The intercept coefficient is indicated by β_0, whereas the linear, squared, and interaction coefficients are represented by β_i, β_{ii}, and β_{ij} (where i = 1,2,3 and j = 1,2,3), respectively. The random error is denoted by ε, and the coded independent variables are X_i and Y_j (El Ouadrhiri et al., 2021).

3. Results and discussion

3.1. FTIR analysis

FTIR spectrum of HC and co-doped hydrochar with iron and copper (Fe/Cu-HC) are shown in Fig. 3. Due to impurities present in the almond shell-derived biomass, the observed modifications in the absorption bands at 480 cm^{-1} and 548 cm^{-1} are more marked. These changes were associated with stretch vibrations of the Cu–O bond (Zhao et al., 2020), the valence bond vibrations of the Fe-O (Adachi et al., 2023); (Gholinejad et al., 2024) . On the Fe/Cu-HC, the C-OH (2922 cm^{-1} and 2853 cm^{-1}) and aromatic C–H group (812 cm^{-1}) were displaced, whereas the C-O functional groups showed a modest rise (Wang et al., 2024). This was attributed to the successful introduction of Fe^{2+} and Cu^{2+}, indicating catalytic reforming and an increase in oxygenated groups during the pyrolysis process (Wan, 2019). The vibration of O–H stretching in alcohols, phenols, and carboxylic acids are responsible for peaks near the absorption band at 3428 cm^{-1}, whereas C = O groups are responsible for those at 1616 cm^{-1}.

3.2. SEM analysis

The co-doping of iron and copper atoms on the hydrochar was confirmed by scanning electron microscopy (SEM) images. As shown in Fig. 4, the surface pores (Fig. 4a) and internal pores (Fig. 4b) of the hydrochar were loaded with iron and copper particles, displaying distinct exposure on the crystalline plane. The Energy-dispersive X-ray spectroscopy (EDS) mappings of the Fe/Cu-HC (Fig. 4c) also reveal and verify the existence of these elements within the catalyst (Gholinejad et al., 1298). EDS analysis of virgin hydrochar and co-doped hydrochar (Fe/Cu-HC) was employed to study the overall chemical composition of the prepared solid catalyst (Fig. 5, Table 2). The results of the analysis show that virgin hydrochar contains negligible amounts of 0.00 % copper (Cu) and 0.01 % iron (Fe) respectively. After pyrolysis, the atomic fractions of the two metals increase by 6.04 % for copper and 8.56 % for iron in the co-doped catalyst, with an atomic ratio of Cu/Fe

Fig. 3. FTIR spectra of virgin hydrochar, Iron-Copper Co-doped hydrochar (Fe/Cu-HC).

almost equal to 1:1, indicating that co-doping of the two metals has been successfully achieved.

3.3. DRX analysis

To identify the main structural differences between hydrochar (HC) and Fe/Cu-HC co-doped catalyst, XRD analysis was carried out (Fig. 6). The results of hydrochar analysis show peaks around 2θ = 15°, 22° and 36°, which have been attributed to cellulose (Raheem et al., 2021). The peaks observed around 36° and 45° indicate a deviation from amorphous carbon. This suggests that the raw biomass has been carbonized in the form of carbon (Zhang et al., 2022). In fact, the peaks associated with cellulose remained at the same positions, but became sharper and developed a more defined shape at higher HTC severity, indicating transformation into disordered carbon (Azzaz et al., 2022). The crystallinity of HC has been improved, probably due to the removal of components such as hemicellulose and lignin from the raw almond shell (Xie et al., 2014).The analysis of the Fe/Cu-HC catalyst shows, in addition to the amorphous carbonaceous plane observed at around 2θ equal to 23°, the presence of characteristic peaks of crystalline planes (1 1 1) (2 2 0) (3 1 1) (4 4 4) (5 1 1) of Fe$_2$O$_3$, observed respectively at values of 2θ at 18.5°, 29.5°, 35.61°, 47.34°, and 79°. These observations suggest the formation of Fe$_2$O$_3$ during the pyrolysis process. Furthermore, we observe peaks corresponding to copper doping in the Fe/Cu-HC catalyst, with values of 2θ = 26.50°, 66.28°, 41.07°, and 50.45° corresponding to lattice planes (0 0 4) (3 1 1) (1 3 1), and (0 6 2) of copper oxides (CuO). As expected, the characteristic Fe$_2$O$_3$ and CuO peaks appeared on Fe/Cu-HC, with low intensity, demonstrating the good doping of the iron and copper metals. The variations observed in the diffraction peaks between HC and Fe/Cu-HC are attributable to the quality of the pyrolysis, which was carried out efficiently (Zhang, 2020).

3.4. BET analysis

Nitrogen (N$_2$) adsorption–desorption isotherms for hydrochar (a) and co-doped catalyst (b) are shown in Fig. 7. According to the original IUPAC classification of physisorption isotherms and associated loops (Thommes, 2015), N$_2$ adsorption–desorption isotherms of our bimetallic catalysts (Fe/Cu-HC) adopt an isotherm type II, which indicates unrestricted monolayer-multilayer adsorption up to high relative pressure. While the presence of an hysteresis type H$_3$ loop prove that the surface of the samples is dominated by non-rigid aggregates of plate-like particles but also in the pore network consisting of macropores which are not completely filled with pore condensate (Oulhakem, 2022), N$_2$ adsorption–desorption analysis with the observation revealed for Scanning electron microscopy. Moreover, the BET surface area obtained is 2.18 m^2. g^{-1} for the Fe/Cu-HC co-doped catalyst and 2.79 m^2. g^{-1} for the hydrochar. The decrease in BET surface area after iron and copper ion impregnation is the result of pore occupancy.

3.5. Effects of monometallic and bimetallic catalysts on MO dye degradation

Fig. 8 depicts the Decolorization efficiency of MO for different prepared catalysts, evaluated under the conditions of the study (Adachi et al., 2023). The degradation efficiency for the Cu-HC, Fe-HC and Fe/Cu-HC catalysts were 66.61 %, 84.11 % and 96 % respectively (Fig. 8a). Compared with the two catalysts (Cu-HC, Fe-HC), the Fe/Cu-HC catalyst showed exceptional degradation efficiency for MO, indicating that the degradation efficiency of the bimetallic Fenton catalyst is superior to that of the monometallic Fenton catalyst. Perhaps copper can participate in Fenton reactions over a wider range of pH values (Nieto-Juarez et al., 2010). Consequently, Cu oxidation can also activate H$_2$O$_2$ decomposition to generate hydroxyl radicals according to equation (3). In order to accelerate the reduction of Fe^{3+} to Fe^{2+} in accordance with the Haber-Weiss mechanism equation (4), this enhances the reaction
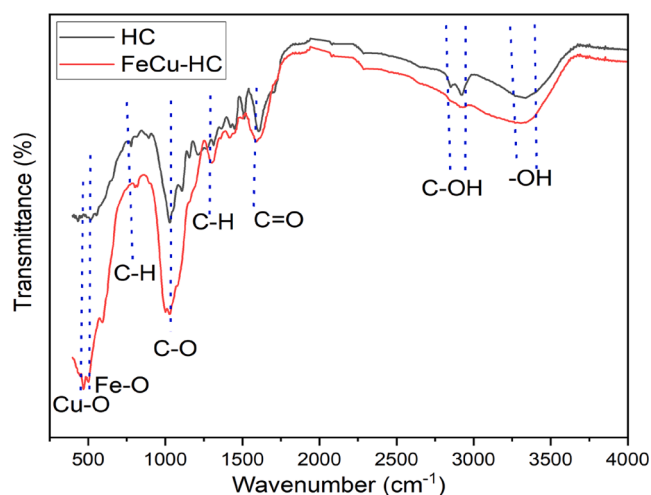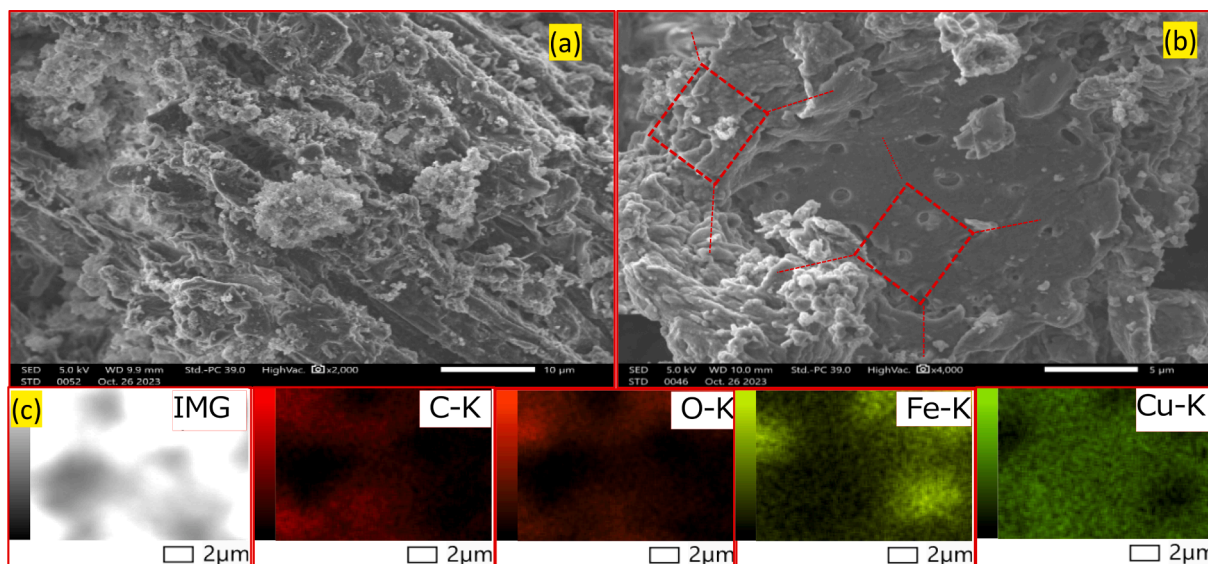
Fig. 4. SEM image of virgin HC (a), hydrochar co-doped Fe/Cu-HC (b), (c) EDS mapping images of Fe/Cu-HC.
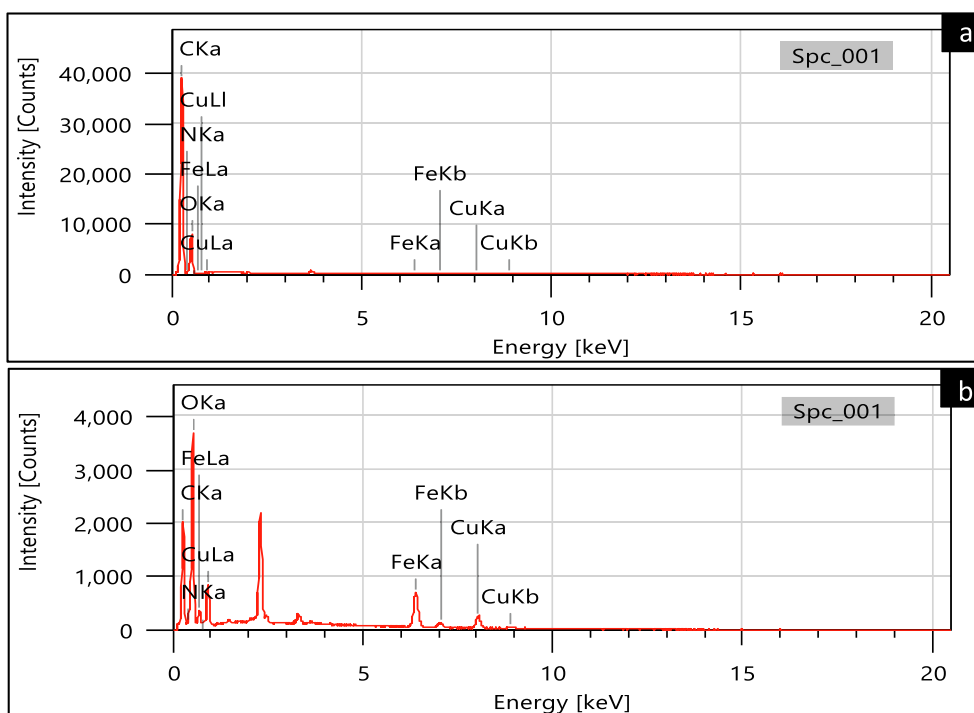

Fig. 5. (a) EDS of virgin HC, (b) Fe/Cu-HC co-doped HC.

Table 2
Experimental ranges and levels of independent variables.

code	Variable	Unit	−1	0	1
X_1	**pH solution**	–	3	4,5	6
X_2	**MO Concentration**	g.ml^{-1}	20	60	100
X_3	**Catalyst mass**	g.l^{-1}	1	1,5	2

rate in the heterogeneous Fenton process, leading to the production of highly reactive free radicals (Xin, 2020).

$$Cu^+ + H_2O_2 Cu^{2+} + OH^· + OH^- \qquad (3)$$

$$Fe^{2+} + H_2O_2 Fe^{3+} + OH^· + OH^- \qquad (4)$$

$$Fe^{3+} + Cu^+ Fe^{2+} + Cu^{2+} \qquad (5)$$

Given that the standard reduction potential of Fe^{3+}/Fe^{2+} is 0.77 V and that of Cu^{2+}/Cu^+ is 0.17 V, the reduction of Fe^{3+} by Cu^+ (Eq. (5)) is thermodynamically favorable, which is beneficial for the Fe^{3+}/Fe^{2+} and Cu^{2+}/Cu^+ redox cycles. Consequently, thanks to the interaction of Fe^{3+}/Fe^{2+} and $Cu+/Cu^{2+}$ pairs, interfacial electron transfer is considerably enhanced in Fe/Cu-HC (Fig. 8b). Based on the above results, the bimetallic Fe/Cu-HC catalyst was selected for further analysis to optimize the conditions of the heterogeneous Fenton process (catalyst mass, pH, methyl orange concentration) with the aim of maximizing dye removal.
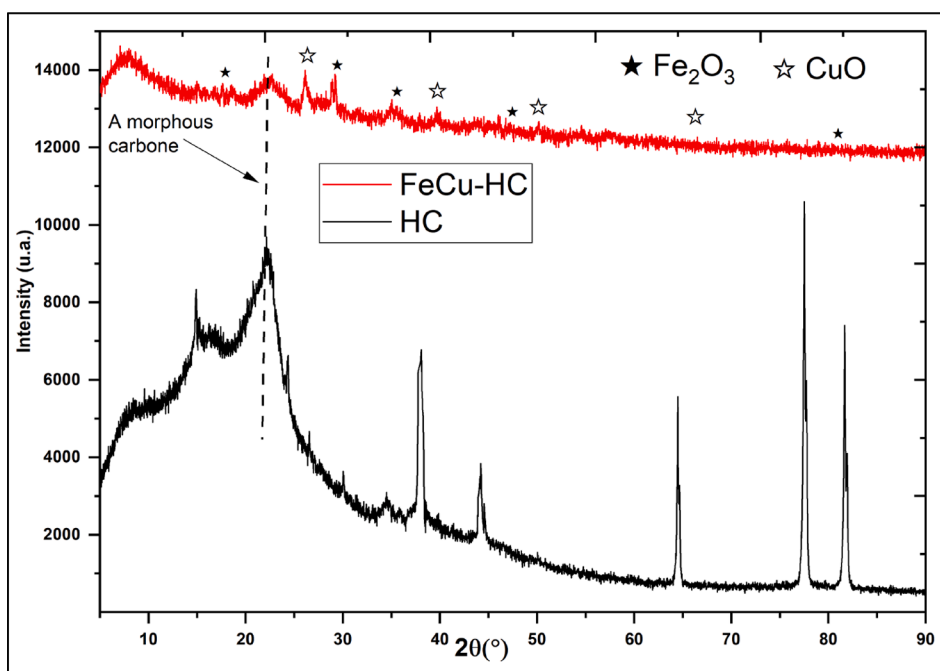
Fig. 6. XRD patterns of virgin HC and co-doped HC with iron and copper Fe/Cu-HC.
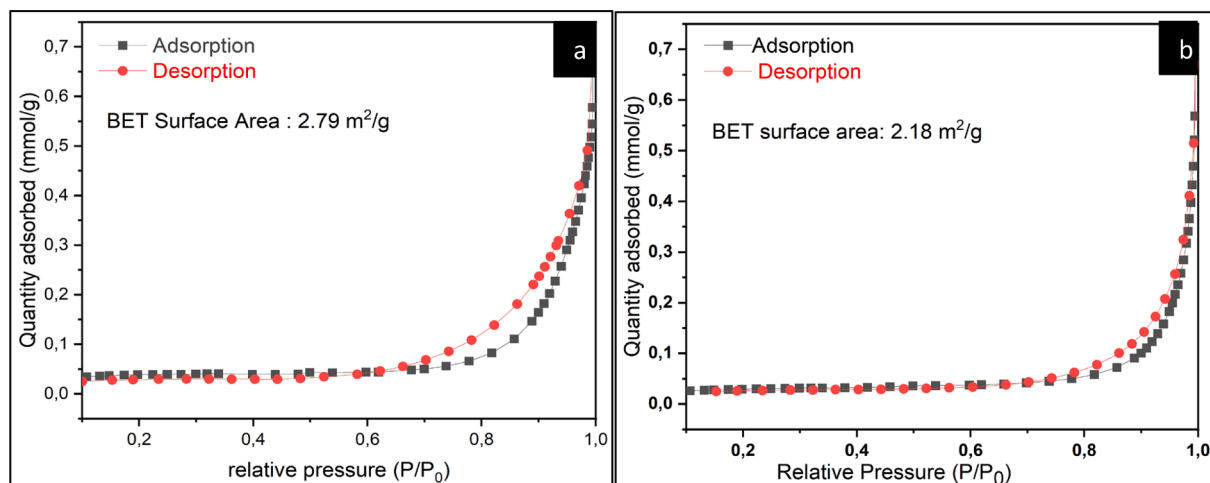

Fig. 7. N_2 physisorption isotherms for (a) HC, (b) co-doped Fe/Cu-HC catalysts.

3.6. Optimization of degradation conditions through statistical modulation

The Fe/Cu-HC catalyst was integrated into the Box-Behnken Design model with a matrix of 15 experiments, aimed at identifying the optimal experimental conditions for an efficient oxidation reaction. The corresponding data are summarized in Table 1S. The BBD analysis was performed in triplicate with central point conditions ($X_1 = 4.5$, $X_2 = 60$ mg. l^{-1}, and $X_3 = 1.5$ g. l^{-1} for pH, MO, and catalyst mass, respectively). The validity of the statistical model tests is evaluated, in part, based on the results of the ANOVA analysis as presented in Table 2S.

The mean square ratio values of the model, the F-*values* shown, and the P-*values* of the confidence interval of the model terms were determined at 95 %, meaning that P-*value* < 5 % guaranteed model significance (El Ouadrhiri, 2023). Consequently, the F (31.98) and P (0.0007) values demonstrate that the statistical validation is very significant. The most significant influence on MO degradation efficiency was determined to be the mass of the Fe/Cu-HC catalyst (F-value = 160.35), which was

followed by the modest influence of MO concentration (F = 7.17), the effect of the solution pH (F-value = 15.62), and the interaction effect between pH and value mass (F = 21.54). But noise might be the only reason for the big-lack-of-fit value 29.06 % could be absent. The model to fit well when there is a non-significant lack of fit. Additionally, the correlation coefficient values $R^2 = 0.98$ and $R_{adj}^2 = 0.95$ show that the created model's applicability is highly predictive and well suited to experimental values (Boutra et al., 2022). In addition, a substantial positive correlation was found between the anticipated and experimental values for MO degradation efficiency by the Fenton heterogeneous process using the Fe/Cu-HC catalyst, as demonstrated by the data displayed in Fig. 9a, 9b. Then, the data point was almost exactly a straight line on the normal probability plot of the residuals. This indicates the efficient performance of the model, confirming its suitability for the degradation of organic pollutants by the heterogeneous Fenton process. Equation (6) represents the second-order polynomial relationship, establishing the regression between the three parameters and the degradation efficiency response.
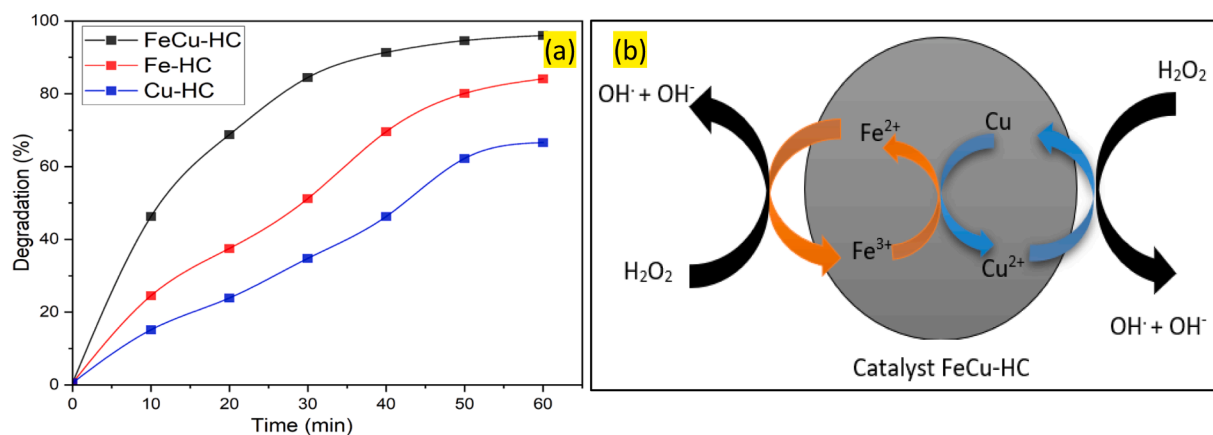
Fig. 8. (a) Degradation efficiency of MO dye by the different prepared catalysts, (b) Schematic illustration of heterogeneous Fenton reactions using Fe/Cu-HC catalysts. Reaction conditions. [MO] = 20 mg. l^{-1}, Catalyst mass = 0.5 g.l^{-1}, [H_2O_2] = 4 mM, pH = 3, T = 35 °C, t = 60 min.
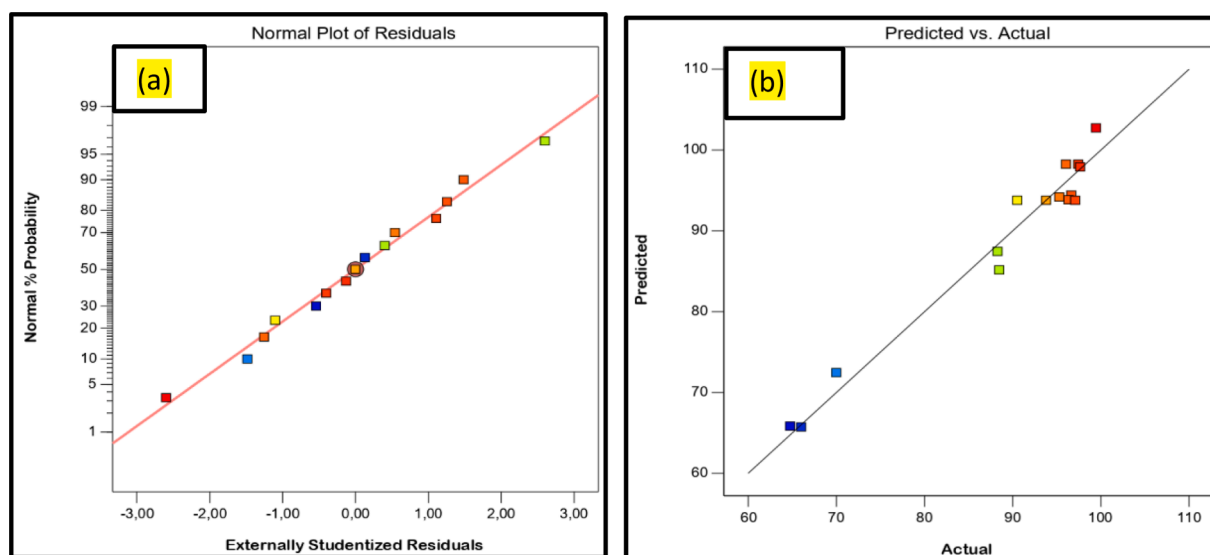

Fig. 9. Representation of normalized residues (a) and comparison between predicted and actual model values (b) for the degradation of MO by a heterogeneous Fenton reaction using the Fe/Cu-HC catalyst.

$$DE(\%) = 94,92 - 3,65X_1 + 2,47X_2 + 11,70X_3 + 1,74X_1X_2$$
$$+ 6,06X_1X_3 - 0,03X_2X_3 + 3,75X_1^2 - 4,08X_2^2 - 10,79X_3^2$$

$$(6)$$

An antagonistic effect is indicated by the presence of a negative sign in front of the observed terms, while a synergistic effect is marked by a positive sign (Khouni et al., 2010). Analysis of the equation reveals the significant impact of catalyst mass on the heterogeneous Fenton reaction, while indicating that the interaction between MO concentration and catalyst mass is not important in this context. Fig. 10a, 10b, and 10c display three-dimensional (3D) response surface plots for MO Decolorization as a function of the solution pH, Fe/Cu-HC catalyst mass, and MO concentration. Fig. 10a shows the effect of pH versus MO concentration on Decolorization efficiency. Increasing MO concentration from 20 to 100 mg. l^{-1} results in a 7.5 % increase in Decolorization efficiency. On the other hand, increasing the pH from 3 to 6 results in a slight decrease in Decolorization rate, of around 8 %. Fig. 10b shows the effect of Fe/Cu-HC catalyst mass as a function of the solution pH. Increasing the catalyst dose from 1 g.l^{-1} to 2 g.l^{-1} results in an increase in the discoloration rate of around 10 %, confirming the importance of mass in the results obtained (Table 1S). On the other hand, increasing the pH of the solution results in a decrease of around 14 %. From Fig. 10c, we can conclude

that in 60 min, with a range of around 1.7 g. l^{-1} for catalyst mass and a high MO concentration of around 80 mg. l^{-1}, a discoloration removal of over 98.5 % can be achieved. However, as their doses are reduced, Decolorization efficiency decreases Fig. 10.

3.7. Numerical optimization

One of the objectives of this study is to achieve maximum Degradation efficiency according to the criteria mentioned in Table 4. The best solution among those determined by the desirability function is the largest value of the D function (0.923) (Figs. 3 and 11), which corresponds to the ratios listed in Table 3.

The prediction point option of the Design Expert software was used to optimize the variables of the heterogeneous Fenton process. Table 3 shows predicted and observed values for MO degradation efficiency under optimal conditions. To validate the response surface methodology (RSM) model based on the Box-Behnken Design under the selected optimization conditions, experiments were conducted for the discoloration of an aqueous solution. It was observed that the experimental degradation efficiency (98.97 %) and the predicted degradation efficiency (99.43 %) showed an error of 0.64 %. Therefore, it was confirmed that equation (2) was capable of accurately calculating the degradation
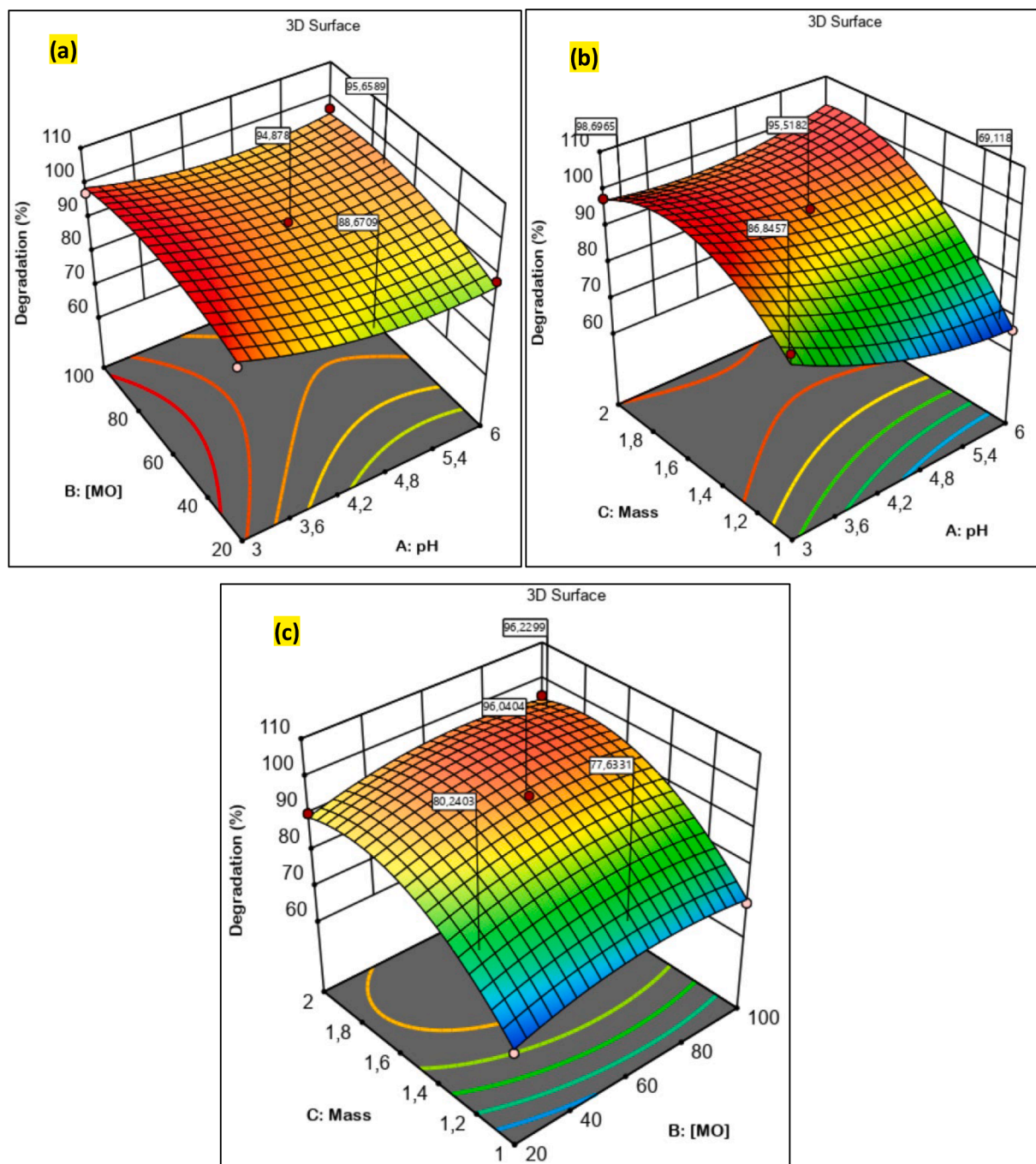
Fig. 10. 3D response surface plots illustrating the impact of the three variables studied on the efficiency of methyl orange degradation by a heterogeneous Fenton reaction with the Fe/Cu-HC catalyst. (For interpretation of the references to color in this figure legend, the reader is referred to the web version of this article.)

rate of the organic pollutant in the aqueous solution.

3.8. Production of hydroxyl radicals (OH⋅)

The degradation of organic matter (OM) was monitored during the tests through UV/Vis scanning across all available wavelengths (Wang et al., 2019); (Guetni et al., 2022) . As illustrated in Fig. 12a, OM exhibited significant absorption of radiation around 464 nm (Adachi, 2022). The signal intensity at 464 nm decreases with increasing oxidation time until no signal is detected within the analyzed range of wavelengths. No other UV/Vis signal was observed in the sample analysis, indicating the absence of any intermediate absorbing radiation at this wavelength. This illustration shows how methyl orange degrades

and loses its color due to the heterogeneous Fenton reaction, which alters the chromophore of the dye (Chen et al., 2008). In order to better understand the mechanism, a trapping experiment was carried out to study the role of OH⋅ radicals in the Fenton reaction. The results presented in Fig. 12b indicate that the addition of n-butanol (10 mM) considerably decreased the efficiency of MO degradation. This suggests that the principal active species in the heterogeneous Fenton process that breaks down MO are OH⋅ radicals (Liu et al., 2013).

3.9. The reusability and stability study

Unlike homogeneous catalysts, the most important feature of heterogeneous catalysts is their ability to be recycled and reused after each
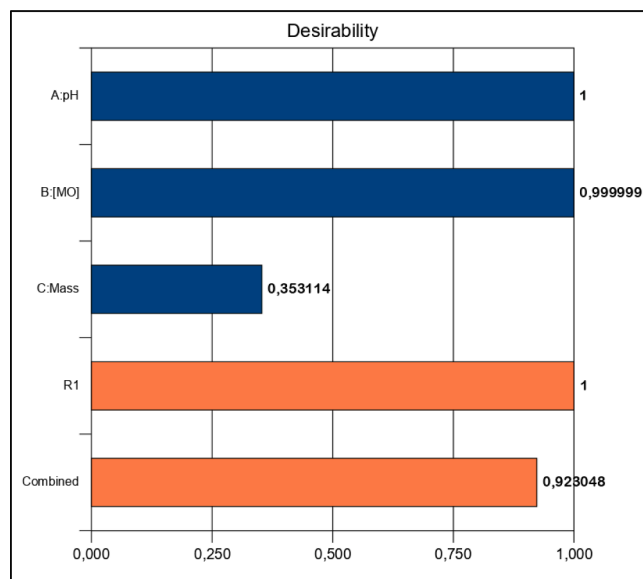
Fig. 11. Optimization desirability function.

Table 3
EDS analysis of the atomic concentrations of elements present in the sample.

Sample	Atomic concentration (%)				Total (%)
	C	**O**	**Fe**	**Cu**	
HC	74.44 ± 0.06	25.55 ± 0.10	0.01 ± 0.00	00 ± 0.01	100
Fe/Cu-HC	45.25 ± 0.17	40.15 ± 0.22	8.56 ± 0.09	6,04 ± 0.12	100

reaction. After each cycle, the Fe/Cu-HC catalyst was recovered, cleaned with distilled water, dried at 100 °C and then calcined for three hours at 400 °C to assess stability (Zhang, et al., 2021). The dye degradation efficiency (DE %) achieved at the end of each experimental run was 98.32 %, 98.16 %, 96.89 %, 96.74 %, and 96.72 %, respectively, as illustrated in Fig. 13. These values indicate that, even after five consecutive experiments, the DE of the organic pollutant remained consistently above 96 %. This consistent performance confirms that the bimetallic Fe/Cu-HC catalyst demonstrates significant stability and is well-suited for reuse in further degradation processes. Furthermore, leakage from the metal active site 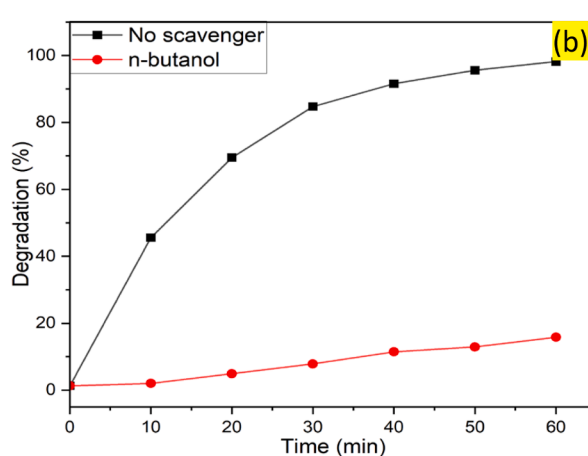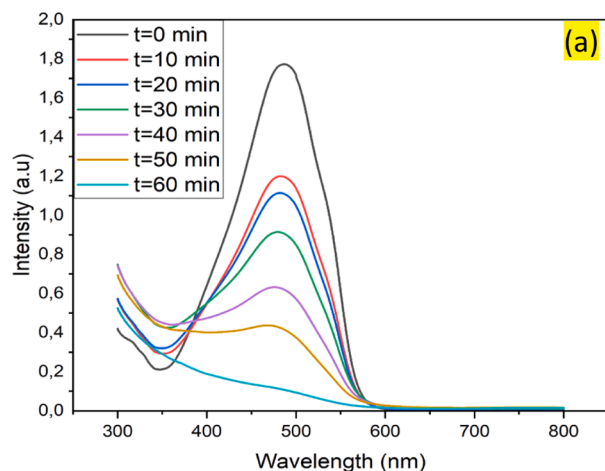and blockage of the active site as a result of the accumulation of the adsorbed intermediate on the catalyst surface could be the cause of the catalyst's slight decrease in oxidizing activity (1.65 %) (Tang and Wang, 2019). Iron and copper leaching from the Fe/Cu-HC catalyst were assessed in treated dye solutions using the ICP-OES method to further confirm this stability (Table 5). After five cycles, the average leaching of iron was limited to 3.42 mg/L and that of copper to 5.02 mg/L, thus demonstrating the HC robust capacity to retain both iron and copper. The FT-IR analysis of the Fe/Cu-HC catalyst
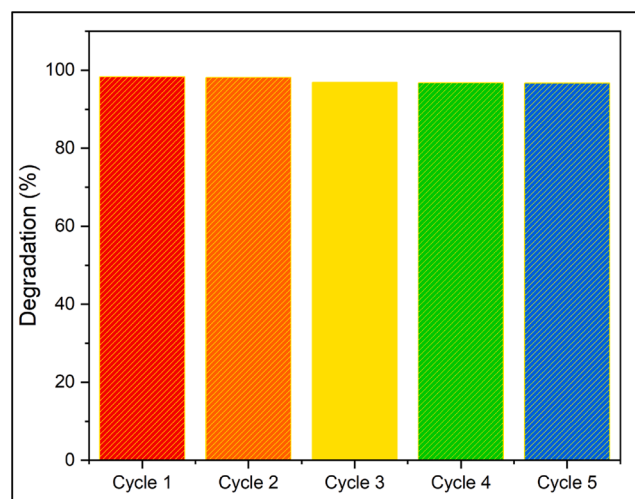

Fig. 13. Methyl Orange degradation efficiency (%) through consecutive cycles in heterogeneous Fenton reaction with Fe/Cu-HC. Reaction conditions. [MO] = 100 mg. l^{-1}, Catalyst mass = 1.65 g.l^{-1}, [H_2O_2] = 4 mM, pH = 6, T = 35 °C, t = 60 min. (For interpretation of the references to color in this figure legend, the reader is referred to the web version of this article.)

Table 4
Experimental and predicted values for MO degradation efficiency (%) under optimal conditions.

Coded Factor	Factor	Value	optimum model prediction	Experimental confirmation of the model
X_1	pH	6	Degradation (%)	Degradation (%)
X_2	[MO] (mg. l^{-1})	100	99,43 %	98,97 %
X_3	catalyst mass (g.l^{-1})	1,65		

Fig. 12. (a) UV–Visible absorption spectra of MO degradation by the Fe/Cu-HC catalyst during the reaction time. (b) MO degradation on the Fe/Cu-HC/H_2O_2 system with or without OH· trapping agent. Reaction conditions: [MO] = 100 mg. l^{-1}, Catalyst mass = 1.65 g.l^{-1}, [H_2O_2] = 4 mM, pH = 6, T = 35 °C, t = 60 min.

Table 5
The leaching of the Fe and Cu under 5 recycle time.

Recycle Times	Iron leaching (mg/l)	copper leaching (mg/l)
1	5,5350	8,711
2	3,3451	7,3693
3	2,7473	3,939
4	2,7256	2,597
5	2,7558	2,487
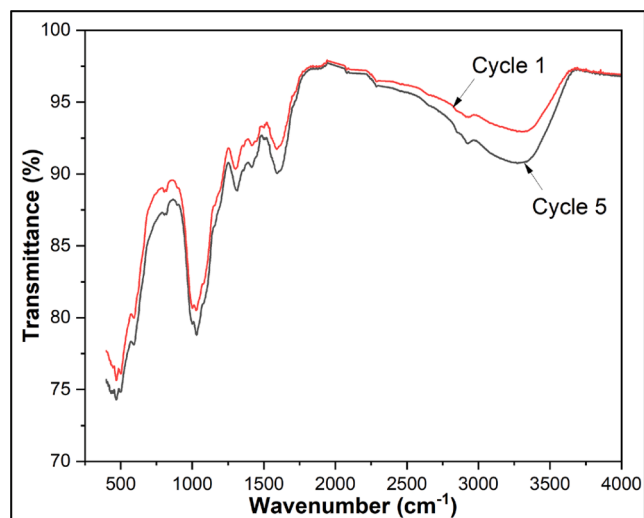
Fig. 14. FTIR spectra of Fe/Cu-HC for cycle 1 and cycle 5.

after the first cycle and the fifth cycle of use is shown in Fig. 14. The FT-IR spectra of the heterogeneous Fenton catalyst Fe/Cu-HC, before and after successive degradation cycles, do not exhibit significant changes in their structure (peaks around 480 cm^{-1} and 548 cm^{-1} which characterize Cu and Fe in the catalyst respectively). This confirms that the catalyst is very stable and can maintain good catalytic activity over an extended period (Ganiyu, et al., 2018).

These results indicate that the Fe/Cu-HC catalyst, as prepared, exhibits excellent stability and recycling performance. Further investigation revealed that the catalyst retains high activity after multiple cycles of use, suggesting its resistance to degradation and wear. This stability is likely attributed to the durable structure of the hydrochar support and the strong interaction between the iron and copper oxides, which prevents the leaching of active metals. However, the preparation and regeneration of bimetallic supports can be costly and complex. Additionally, bimetallic catalysts are highly sensitive to the pH of the medium, requiring precise pH control to maintain optimal catalytic activity.

Table 6 compares the efficiency of the Fe/Cu-HC catalyst in the degradation of organic matter (OM) with the results of a previous study. This comparison considers the treatment of synthetic dyes by the heterogeneous Fenton process, employing various solid catalysts and applying them under various optimum conditions (pH, H_2O_2 dose, organic pollutant concentration, catalyst mass, reaction time). In our study, we observed that the catalyst we developed is highly effective in degrading organic matter, achieving a degradation rate of 98.97 %. This performance significantly surpasses that of other catalysts reported in the literature. Notably, these results were obtained using a relatively small amount of catalyst, in a solution with a neutral pH and a high concentration of organic pollutants. This demonstrates the robustness and versatility of the Fe/Cu-HC catalyst's efficiency, even under diverse environmental conditions. These results indicate that the various catalytic systems react in distinct ways, complicating the generalization of optimal conditions for maximizing organic matter degradation from one

Table 6
Comparison of organic matter degradation by the heterogeneous Fenton process using different catalysts under various optimum conditions.

Catalyst	Optimal reaction conditions	Degradation efficiency	Reference
Fe/Cu-MMT	Catalyst mass = 1.5 g. l^{-1}, [RhB] = 100 mg. l^{-1} [H_2O_2] = 5 mmol. l^{-1}, t = 90 min, pH = 7	87.9 %	(Zhang, et al., 2021)
CuFe$_2$O$_4$	catalyst mass = 0.1 g. l^{-1}, [MB] = 50 mg. l^{-1}, [H_2O_2] = 0.5 mmol/l, t = 25 min, pH = 3.2	74 %	(Qin et al., 2018)
CuFeZSM-5	Catalyst mass = 0.3 g. l^{-1}, [R6G] = 100 mg. l^{-1} [H_2O_2] = 40 mmol. l^{-1}, t = 45 min, pH = 3.4	100 %	(Dükkanci et al., 2010)
Pepper stalks BC/CuFeO$_2$	Catalyst mass = 0.5 g. l^{-1}, [TC] = 20 mg. l^{-1}, [H_2O_2] = 50 mmol.l^{-1}, t = 300 min, pH = 6.3	100 %	(Xin, 2020)
Cu-Fe@biochar	Catalyst mass = 15 mg. l^{-1}, [MB] = 50 mg. l^{-1} [H_2O_2] = 16 mM mmol. l^{-1}, t = 20 min pH = 2.5	100 %	(Liu et al., 2022)
Fe/Cu-HC	Catalyst mass = 1.65 g. l^{-1}, [MO] = 100 mg. l^{-1} [H_2O_2] = 4 mmol/l, t = 60 min, pH = 6	98.97 %	This study

system to another.

4. Conclusion

In this study, a novel catalyst, Fe/Cu-HC, was developed by doping iron (Fe) and copper (Cu) into hydrochar (HC) derived from almond shells (AS) through a hydrothermal carbonization process. This process involves the hydrothermal treatment of almond shells to produce hydrochar, which is then impregnated with iron and copper ions. The hydrothermal carbonization results in a porous carbon structure, promoting uniform dispersion of the metals and enhancing the catalytic properties of the material. The impact of the three experimental parameters on the degradation rate of methyl orange was assessed, using a Box-Behnken design coupled with response surface methodology. Under optimal conditions (catalyst mass = 1.65 g.l^{-1}, [MO] = 100 g.l^{-1}, pH = 6), a degradation rate of 98.97 % for MO was achieved through the heterogeneous Fenton process. Hydroxyl radicals (OH·) play a dominant role in the degradation of methyl orange by the heterogeneous Fenton process. The bimetallic Fe/Cu-HC catalyst demonstrated stable activity over 5 usage cycles with minimal loss of efficiency (less than 5 %). This study provided a simple and low-cost technical approach for preparing a highly efficient bimetallic catalyst based on hydrochar for the treatment of wastewater contaminated with an azoic dye. Future research will focus on the application of biomass-derived catalysts in wastewater treatment, including the degradation of other pollutants, process optimization, and cost assessment.

CRediT authorship contribution statement

Abderrazzak Adachi: Writing – original draft, Visualization, Validation, Supervision, Software, Resources, Methodology, Investigation, Funding acquisition, Formal analysis, Data curation, Conceptualization. **Faiçal El Ouadrhiri:** Writing – original draft, Visualization, Validation, Supervision, Software, Methodology, Investigation, Data curation, Conceptualization. **Ebraheem Abdu Musad Saleh:** Writing – original draft, Visualization, Supervision, Methodology. **Fatima Moussaoui:** Formal analysis, Data curation, Conceptualization. **Raed H. Althomali:** Validation, Resources, Methodology, Investigation. **Soukaina El**

Appendix A. Supplementary data

Supplementary data to this article can be found online at https://doi.org/10.1016/j.arabjc.2024.105862.

References

Adachi, A., et al., 2022. Decolorization and Degradation of Methyl Orange Azo Dye in Aqueous Solution by the Electro Fenton Process: Application of Optimization. Catalysts 12 (6), 1–12. https://doi.org/10.3390/catal12060665.

Adachi, A., et al., 2023. Cactus and Holm Oak Acorn for Efficient Textile Wastewater Treatment by Coagulation-Flocculation Process Optimization Using Box-Benhken Design. J. Ecol. Eng. 24 (6), 315–328. https://doi.org/10.12911/22998993/162784.

Adachi, A., El, F., Ebraheem, O., Musad, A., Raed, S., 2023. Iron - doped catalyst synthesis in heterogeneous Fenton like process for dye degradation and removal : optimization using response surface methodology. SN Appl. Sci. https://doi.org/10.1007/s42452-023-05543-0.

Adachi, A., El Ouadrhiri, F., El Manssouri, I., Moussaoui, F., El Bourachdi, S., Lahkimi, A., 2023. Removal of Dyes by Adsorption Process Using Date Pits as Material Environmentally Friendly. Ecol. Eng. Environ. Technol. 24 (8), 181–193. https://doi.org/10.12912/27197050/171494.

Alcazar-Ruiz, A., Villardon, A., Dorado, F., Sanchez-Silva, L., 2023. Hydrothermal carbonization coupled with fast pyrolysis of almond shells: Valorization and production of valuable chemicals. Waste Manag. 169 (March), 112–124. https://doi.org/10.1016/j.wasman.2023.07.004.

Azzaz, A.A., Ghimbeu, C.M., Jellai, S., El-Bassi, L., Jeguirim, M., 2022. Olive Mill by-Products Thermochemical Conversion via Hydrothermal Carbonization and Slow Pyrolysis: Detailed Comparison between the Generated Hydrochars and Biochars Characteristics. Processes 10 (2), pp. https://doi.org/10.3390/pr10020231.

Babar, M., et al., 2022. Comparative study of ozonation and ozonation catalyzed by Fe-loaded biochar as catalyst to remove methylene blue from aqueous solution. Chemosphere 307 (P1), 135738. https://doi.org/10.1016/j.chemosphere.2022.135738.

Baldrian, P., et al., 2006. Decolorization of synthetic dyes by hydrogen peroxide with heterogeneous catalysis by mixed iron oxides. Appl. Catal. B Environ. 66 (3–4), 258–264. https://doi.org/10.1016/j.apcatb.2006.04.001.

T. Binh, C. Dong, C. P. Huang, C. Chen, S. Hsieh, and S. Hsieh, "Journal of Environmental Chemical Engineering Fe-Cu bimetallic catalyst for the degradation of hazardous organic chemicals exempli fi ed by methylene blue in Fenton-like reaction," *J. Environ. Chem. Eng.*, vol. 8, no. 5, p. 104139, 2020, doi: 10.1016/j.jece.2020.104139.

Boutra, B., Sebti, A., Trari, M., 2022. Response surface methodology and artificial neural network for optimization and modeling the photodegradation of organic pollutants in water. Int. J. Environ. Sci. Technol. 19 (11), 11263–11278. https://doi.org/10.1007/s13762-021-03875-1.

Chen, Y.P., Liu, S.Y., Yu, H.Q., Yin, H., Li, Q.R., 2008. Radiation-induced degradation of methyl orange in aqueous solutions. Chemosphere 72 (4), 532–536. https://doi.org/10.1016/j.chemosphere.2008.03.054.

Y. Ding et al. Deep mineralization of bisphenol A by catalytic peroxymonosulfate activation with nano CuO/Fe3O4 with strong Cu-Fe interaction Chem. Eng. J. 384 October 2020 2019, p. 123378 10.1016/j.cej.2019.123378.

Duan, P., et al., 2020. Enhanced degradation of clothianidin in peroxymonosulfate/catalyst system via core-shell FeMn @ N-C and phosphate surrounding. Appl. Catal. B Environ. vol. 267, no. January, 118717 https://doi.org/10.1016/j.apcatb.2020.118717.

Duan, X., Sun, H., Ao, Z., Zhou, L., Wang, G., Wang, S., 2016. Unveiling the active sites of graphene-catalyzed peroxymonosulfate activation. Carbon n. y. 107, 371–378. https://doi.org/10.1016/j.carbon.2016.06.016.

M. Dükkanci G. Gündüz S. Yilmaz R. V. Prihod`ko, Heterogeneous Fenton-like degradation of Rhodamine 6G in water using CuFeZSM-5 zeolite catalyst prepared by hydrothermal synthesis J. Hazard. Mater. 181 1–3 2010 343 350 10.1016/j.jhazmat.2010.05.016.

El Ouadrhiri, F., et al., 2023. Acid assisted-hydrothermal carbonization of solid waste from essential oils industry: Optimization using I-optimal experimental design and removal dye application. Arab. J. Chem. 16 (8), pp. https://doi.org/10.1016/j.arabjc.2023.104872.

El Ouadrhiri, F., et al., May 2023. Nitrogen and phosphorus co-doped carbocatalyst for efficient organic pollutant removal through persulfate-based advanced oxidation processes. J. Saudi Chem. Soc. 27 (3), 101648 https://doi.org/10.1016/j.jscs.2023.101648.

El Ouadrhiri, F., Elyemni, M., Lahkimi, A., Lhassani, A., Chaouch, M., Taleb, M., 2021. Mesoporous Carbon from Optimized Date Stone Hydrochar by Catalytic Hydrothermal Carbonization Using Response Surface Methodology: Application to Dyes Adsorption. Int. J. Chem. Eng. 2021 https://doi.org/10.1155/2021/5555406.

Fu, D., Agustiono, T., Li, H., Wang, H., Wang, Y., Li, Q., 2021. Co-oxidative removal of arsenite and tetracycline based on a heterogeneous Fenton-like reaction using iron nanoparticles-impregnated biochar ☆. Environ. Pollut. vol. 290, no. January, 118062 https://doi.org/10.1016/j.envpol.2021.118062.

S. O. Ganiyu *et al.*, "Application of least squares support vector regression and linear multiple regression for modeling removal of methyl orange onto tin oxide nanoparticles loaded on activated carbon and activated carbon prepared from Pistacia atlantica wood," *Appl. Catal. B Environ.*, vol. 404, no. April 2018, pp. 672–680, 2016, doi: 10.1016/j.apcatb.2019.01.026.

Genli, N., Kutluay, S., Baytar, O., Şahin, Ö., 2022. Preparation and characterization of activated carbon from hydrochar by hydrothermal carbonization of chickpea stem: an application in methylene blue removal by RSM optimization. Int. J. Phytoremediation 24 (1), 88–100. https://doi.org/10.1080/15226514.2021.1926911.

Gholinejad, M., Bashirimousavi, S., Sansano, J.M., 2024. Novel magnetic bimetallic AuCu catalyst for reduction of nitroarenes and degradation of organic dyes. Sci. Rep. 1–16. https://doi.org/10.1038/s41598-024-56559-4.

M. Gholinejad, M. Iranpanah, and S. Karimi, "Cysteine and ionic liquid modified magnetic nanoparticles supported RuCu as a new bimetallic catalyst in reduction reactions," vol. 1298, no. August 2023, 2024, doi: 10.1016/j.molstruc.2023.137100.

Guetni, I., Belaiche, M., Ferdi, C.A., Oulhakem, O., Alaoui, K.B., Naimi, Z., 2022. Engineering the photocatalytic efficiency of nanoscale TiO2 anatase with doped (Nd/Y) and co-doped (Nd-Y/Nd-Sm) lanthanides to decompose the azo dye orange G under UV-VIS irradiation. New J. Chem. 46 (21), 10162–10183. https://doi.org/10.1039/d2nj01167k.

Hashemian, S., Salari, K., Yazdi, Z.A., 2014. Preparation of activated carbon from agricultural wastes (almond shell and orange peel) for adsorption of 2-pic from aqueous solution. J. Ind. Eng. Chem. 20 (4), 1892–1900. https://doi.org/10.1016/j.jiec.2013.09.009.

Huang, Q., et al., 2021. Malachite green degradation by persulfate activation with CuFe2O4@biochar composite: Efficiency, stability and mechanism. J. Environ. Chem. Eng. 9 (4), 105800 https://doi.org/10.1016/j.jece.2021.105800.

Hussain, S., Aneggi, E., Trovarelli, A., Goi, D., 2022. Removal of Organics from Landfill Leachate by Heterogeneous Fenton-like Oxidation over Copper-Based Catalyst. Catalysts 12 (3), 1–17. https://doi.org/10.3390/catal12030338.

Khan, H., et al., 2023. Multiple design and modelling approaches for the optimisation of carbon felt electro-Fenton treatment of dye laden wastewater. Chemosphere vol. 338, no. June, 139510. https://doi.org/10.1016/j.chemosphere.2023.139510.

Khouni, I., Marrot, B., Ben Amar, R., 2010. Decolourization of the reconstituted dye bath effluent by commercial laccase treatment: Optimization through response surface methodology. Chem. Eng. J. 156 (1), 121–133. https://doi.org/10.1016/j.cej.2009.10.007.

Ledesma, B., Olivares-Marín, M., Álvarez-Murillo, A., Roman, S., Nabais, J.M.V., 2018. Method for promoting in-situ hydrochar porosity in hydrothermal carbonization of almond shells with air activation. J. Supercrit. Fluids 138 (April), 187–192. https://doi.org/10.1016/j.supflu.2018.04.018.

Li, Y., et al., 2022. Journal of Environmental Chemical Engineering Preparation of cobalt / hydrochar using the intrinsic features of rice hulls for dynamic carbamazepine degradation via efficient PMS activation. J. Environ. Chem. Eng. 10 (6), 108659 https://doi.org/10.1016/j.jece.2022.108659.

Li, J., Li, M., Sun, H., Ao, Z., Wang, S., Liu, S., 2020. Understanding of the Oxidation Behavior of Benzyl Alcohol by Peroxymonosulfate via Carbon Nanotubes Activation. ACS Catal. 10 (6), 3516–3525. https://doi.org/10.1021/acscatal.9b05273.

Li, Z., Lyu, J., Ge, M., 2018. Synthesis of magnetic Cu/CuFe2O4 nanocomposite as a highly efficient Fenton-like catalyst for methylene blue degradation. J. Mater. Sci. 53 (21), 15081–15095. https://doi.org/10.1007/s10853-018-2699-0.

Liu, X., Wang, X., Yang, W., Yuan, F., Wang, B., Peng, Q., 2022. Impregnating biochar with Fe and Cu by bioleaching for fabricating catalyst to activate H2O2. Appl. Microbiol. Biotechnol. 106 (5), 2249–2262. https://doi.org/10.1007/s00253-022-11853-x.

Liu, J., Zhang, G., Yu, J.C., Guo, Y., 2013. In situ synthesis of Zn2GeO4 hollow spheres and their enhanced photocatalytic activity for the degradation of antibiotic metronidazole. Dalt. Trans. 42 (14), 5092–5099. https://doi.org/10.1039/c2dt32623j.

Lousada, C.M., Johansson, A.J., Brinck, T., Jonsson, M., 2012. Mechanism of H2O2 decomposition on transition metal oxide surfaces. J. Phys. Chem. C 116 (17), 9533–9543. https://doi.org/10.1021/jp300255h.

Methods, H., 2010. "chemical Product and Process Modeling Search for Optimal Design of Multiproduct Batch Plants under Uncertain Demand Using Gaussian Process Modeling Solved by Heuristics Methods Search for Optimal Design of Multiproduct Batch Plants under Uncertain Demand Using Gaussian Process Modeling Solved by Heuristics Methods *" 5 (1), pp.

Mirdamadi, S.H., Khodaei, M., Valanezhad, A., Watanabe, I., Nejatidanesh, F., Savabi, O., 2022. Effect of post heat treatment on surface properties of hydrogen peroxide (H2O2) treated titanium. J. Mater. Res. Technol. 18, 584–590. https://doi.org/10.1016/j.jmrt.2022.02.095.

Z. Naghshbandi and M. Gholinejad, "New recyclable Co-based trimetallic zeolite imidazolate framework (Cu-Ni @ ZIF-67) as an efficient catalyst for different reduction reactions," vol. 243, no. April, 2023, doi: 10.1016/j.poly.2023.116523.

Nieto-Juarez, J.I., Pierzchla, K., Sienkiewicz, A., Kohn, T., 2010. Inactivation of MS2 coliphage in Fenton and Fenton-like systems: Role of transition metals, hydrogen

peroxide and sunlight. Environ. Sci. Technol. 44 (9), 3351–3356. https://doi.org/10.1021/es903739f.

Oginni, O., Singh, K., Oporto, G., Dawson-Andoh, B., McDonald, L., Sabolsky, E., 2019. Influence of one-step and two-step KOH activation on activated carbon characteristics. Bioresour. Technol. Reports vol. 7, no. April, 100266. https://doi.org/10.1016/j.biteb.2019.100266.

Oulhakem, O., et al., 2022. One-step immobilization of tungsten oxide on microporous silica surface as a photocatalyst for water pollutant removal. Microporous Mesoporous Mater. vol. 335, no. March, 111784 https://doi.org/10.1016/j.micromeso.2022.111784.

P. Peerakiatkhajohn, T. Butburee, J. Sul, and S. Thaweesak, "Efficient and Rapid Photocatalytic Degradation of Methyl Orange Dye Using Al / ZnO Nanoparticles," pp. 1–13, 2021.

Pourali, P., Fazlzadeh, M., Aaligadri, M., Dargahi, A., Poureshgh, Y., Kakavandi, B., 2022. Enhanced three-dimensional electrochemical process using magnetic recoverable of Fe3O4@GAC towards furfural degradation and mineralization. Arab. J. Chem. 15 (8), 103980 https://doi.org/10.1016/j.arabjc.2022.103980.

Qin, Q., Liu, Y., Li, X., Sun, T., Xu, Y., 2018. Enhanced heterogeneous Fenton-like degradation of methylene blue by reduced CuFe2O4. RSC Adv. 8 (2), 1071–1077. https://doi.org/10.1039/c7ra12488k.

Queirós, C.S.G.P., et al., . "Characterization of walnut, almond, and pine nut shells regarding chemical composition and extract composition", no. Mill.

Rahdar, S., Igwegbe, C.A., Ghasemi, M., Ahmadi, S., 2019. Degradation of aniline by the combined process of ultrasound and hydrogen peroxide (US/H 2 O 2). MethodsX 6, 492–499. https://doi.org/10.1016/j.mex.2019.02.033.

A. Raheem, Q. He, L. Ding, W. Dastyar, and G. Yu, "Evaluating performance of pyrolysis and gasification processes of agriculture residues-derived hydrochar: Effect of hydrothermal carbonization," J. Clean. Prod., vol. 338, no. June 2021, p. 130578, 2022, doi: 10.1016/j.jclepro.2022.130578.

Rehan, A.I., et al., 2023. Improving toxic dye removal and remediation using novel nanocomposite fibrous adsorbent. Colloids Surfaces A Physicochem. Eng. Asp. vol. 673, no. May, 131859 https://doi.org/10.1016/j.colsurfa.2023.131859.

Roman, F.F., Diaz De Tuesta, J.L., Praça, P., Silva, A.M.T., Faria, J.L., Gomes, H.T., 2021. Hydrochars from compost derived from municipal solid waste: Production process optimization and catalytic applications. J. Environ. Chem. Eng. 9 (1), 1–9. https://doi.org/10.1016/j.jece.2020.104888.

D. H. S. Santos, J. L. S. Duarte, J. Tonholo, L. Meili, and C. L. P. S. Zanta, "Saturated activated carbon regeneration by UV-light, H2O2 and Fenton reaction," Sep. Purif. Technol., vol. 250, no. March, p. 117112, 2020, doi: 10.1016/j.seppur.2020.117112.

Shi, X., Tian, A., You, J., Yang, H., Wang, Y., Xue, X., 2018. Degradation of organic dyes by a new heterogeneous Fenton reagent - Fe2GeS4 nanoparticle. J. Hazard. Mater. 353 (January), 182–189. https://doi.org/10.1016/j.jhazmat.2018.04.018.

Song, H., Li, Q., Ye, Y., Pan, F., Zhang, D., Xia, D., 2021. Degradation of cephalexin by persulfate activated with magnetic loofah biochar: Performance and mechanism. Sep. Purif. Technol. vol. 272, no. May, 118971 https://doi.org/10.1016/j.seppur.2021.118971.

Tang, J., Wang, J., 2019. MOF-derived three-dimensional flower-like FeCu@C composite as an efficient Fenton-like catalyst for sulfamethazine degradation. Chem. Eng. J. vol. 375, no. April, 122007 https://doi.org/10.1016/j.cej.2019.122007.

Tang, J., Wang, J., 2020. Chemosphere Iron-copper bimetallic metal-organic frameworks for ef fi cient Fenton- like degradation of sulfamethoxazole under mild conditions. Chemosphere 241, 125002. https://doi.org/10.1016/j.chemosphere.2019.125002.

Tao, X., Yang, C., Wei, Z., Huang, L., Chen, J., Cong, W., 2019. Synergy between Fenton process and DBD for methyl orange degradation. Mater. Res. Bull. vol. 120, no. June, 110581 https://doi.org/10.1016/j.materresbull.2019.110581.

Thommes, M., et al., 2015. Physisorption of gases, with special reference to the evaluation of surface area and pore size distribution (IUPAC Technical Report). Pure Appl. Chem. 87 (9–10), 1051–1069. https://doi.org/10.1515/pac-2014-1117.

Wan, Z., et al., 2019. A sustainable biochar catalyst synergized with copper heteroatoms and CO2 for singlet oxygenation and electron transfer routes. Green Chem. 21 (17), 4800–4814. https://doi.org/10.1039/c9gc01843c.

Wang, C., Cao, Y., Wang, H., 2019. Copper-based catalyst from waste printed circuit boards for effective Fenton-like discoloration of Rhodamine B at neutral pH. Chemosphere 230, 278–285. https://doi.org/10.1016/j.chemosphere.2019.05.068.

J. Wang, Z. Xi, B. Niu, R. Gao, and Z. Xu, "Catalytic Pyrolysis of Waste-Printed Circuit Boards Using a Cu / Fe Bimetal Synergistic Effect to Enhance Debromination," pp. 1–13, 2024.

Wang, C., Huang, R., Sun, R., 2020. Green one-spot synthesis of hydrochar supported zero-valent iron for heterogeneous Fenton-like discoloration of dyes at neutral pH. J. Mol. Liq. 320, 114421 https://doi.org/10.1016/j.molliq.2020.114421.

Xie, M., Chen, W., Xu, Z., Zheng, S., Zhu, D., 2014. Adsorption of sulfonamides to demineralized pine wood biochars prepared under different thermochemical conditions. Environ. Pollut. 186, 187–194. https://doi.org/10.1016/j.envpol.2013.11.022.

Y. Xie et al. Applied Surface Science Photosynergetic bimetallic Fe-Cu codoped melem polymer for boosting Fenton-like catalytic performance : Insights into the enhancement mechanism Appl. Surf. Sci. 612 November 2023 2022, p. 155899 10.1016/j.apsusc.2022.155899.

Xin, S., et al., 2020. High efficiency heterogeneous Fenton-like catalyst biochar modified CuFeO2 for the degradation of tetracycline: Economical synthesis, catalytic performance and mechanism. Appl. Catal. B Environ. 280 (January), 2021. https://doi.org/10.1016/j.apcatb.2020.119386.

Zhang, X., et al., 2020. Characterization and sulfonamide antibiotics adsorption capacity of spent coffee grounds based biochar and hydrochar. Sci. Total Environ. 716 https://doi.org/10.1016/j.scitotenv.2020.137015.

Zhang, C., Yang, W., Chen, W.H., Ho, S.H., Pétrissans, A., Pétrissans, M., 2022. Effect of torrefaction on the structure and reactivity of rice straw as well as life cycle assessment of torrefaction process. Energy 240. https://doi.org/10.1016/j.energy.2021.122470.

X. Zhang et al. Efficient and stable iron-copper montmorillonite heterogeneous Fenton catalyst for removing Rhodamine B Chem. Phys. Lett. vol. 776, no. February 2021 138673 10.1016/j.cplett.2021.138673.

Zhao, Y., Song, M., Cao, Q., Sun, P., Chen, Y., Meng, F., 2020. The superoxide radicals' production via persulfate activated with CuFe2O4@Biochar composites to promote the redox pairs cycling for efficient degradation of o-nitrochlorobenzene in soil. J. Hazard. Mater. vol. 400, no. May, 122887 https://doi.org/10.1016/j.jhazmat.2020.122887.